Cement and Concrete Research 39 (2009) 345–352

Contents lists available at ScienceDirect

Cement and Concrete Research

journal homepage: http://ees.elsevier.com/CEMCON/default.asp

Correlation of hollow and solid cylinder dynamic pressurization tests for measuring permeability

Christopher A. Jones, Zachary C. Grasley *

Texas A&M University, TAMU 3135, College Station, Texas 77843, United States

ARTICLE INFO

Article history:
Received 14 May 2008
Accepted 24 December 2008

Keywords:
Degradation
Durability
Permeability
Transport properties
Poromechanics

ABSTRACT

An experimental apparatus and analytical derivation are developed for quantifying the permeability of cementitious materials using dynamic pressurization of a hollow cylinder. Experimental results from the newly developed hollow dynamic pressurization technique for measuring permeability are then compared to results obtained using the solid dynamic pressurization test. The measured permeabilities obtained from testing Vycor® glass and hardened cement paste indicate close agreement between the two test methods, which supports the validation of the hollow dynamic pressurization test as an accurate and repeatable method for measuring the permeability of cementitious materials. Three different pore fluids with widely varying viscosities were tested, each yielding equivalent intrinsic permeabilities. Additionally, the permeability values from this study agree reasonably well with relevant values presented in the recent literature.

1. Introduction

The susceptibility of concrete to various forms of moisture related damage is a primary challenge facing the concrete construction industry. Alkali-aggregate reactivity, sulfate attack, corrosion of reinforcing steel, and freeze–thaw damage are examples of concrete infrastructure problems that are dependent on moisture transport within the pore network of concrete. Despite the importance of moisture transport in cementitious materials, no widely accepted technique for quantifying material permeability has been developed [1]. To this end, the authors aim to validate a newly developed hollow (cylinder) dynamic pressurization (HDP) technique for measuring permeability by comparing results with the solid (cylinder) dynamic pressurization (SDP) technique [2,3].

Permeability, the relative resistance of a material to fluid transmission under a pressure gradient, is a viable technique for characterizing the durability of concrete, though traditional methods of measuring this property have limitations. A typical "flow-through" permeability test would involve applying a differential pressure head to a sample and measuring the amount of fluid that passes through the sample in a specified period of time under steady-state conditions. Ye demonstrates a typical flow-through measurement apparatus, which tests several samples simultaneously [4]. The chief drawback of current flow-through permeability measurement techniques is the large amount of time required to run a single test. Specimens with low permeability can take days to reach equilibrium flow (steady-state), which is required before accurate measurement can begin [5]. Traditional methods of testing concrete permeability can take as long as several weeks to run and show high variability and limited repeatability [6]. Furthermore, the long test duration precludes permeability testing at early ages since the specimen being tested would age significantly during the test. To address the problem of slow flow rates, increased differential pressures are often employed to increase flow rates. With the increased pressure often comes a host of other problems such as specimen damage or leaking around seals [7].

Novel approaches based on poromechanics have recently been developed in an effort to more rapidly and accurately measure the permeability of cementitious materials. Various examples are discussed by Scherer et al. [7] including beam bending [8], thermo-permeametry [9], and dynamic pressurization [3]. The latter is of great interest because it seems to have the fewest practical limitations and therefore could potentially be used outside of research to aid the construction process by qualifying trial mixtures for use, by providing a means for quality assurance/quality control, or to monitor curing. The potential exists to use either cast specimens or cores.

The dynamic pressurization method involves the rapid hydrostatic pressurization of a cylindrical specimen within a pressure cell. The cylinder responds with a volumetric contraction that is dependent on the bulk modulus of the specimen and the pore fluid [3]. Then, as fluid flows into the pores of the specimen, the cylinder expands at a rate that is related to the rate of fluid flow in the pore network. Scherer shows a schematic representation of the response of the sample to a step pressurization in Fig. 1 of [3]. By measuring the strain-time history, the permeability of the specimen can be obtained in a reasonable amount of time.

One disadvantage of the dynamic pressurization test is the difficulty of testing specimens with high permeability; for such

* Corresponding author. Tel.: +1 979 845 9961.
E-mail address: zgrasley@civil.tamu.edu (Z.C. Grasley).

0008-8846/$ – see front matter © 2009 Elsevier Ltd. All rights reserved.
doi:10.1016/j.cemconres.2008.12.010

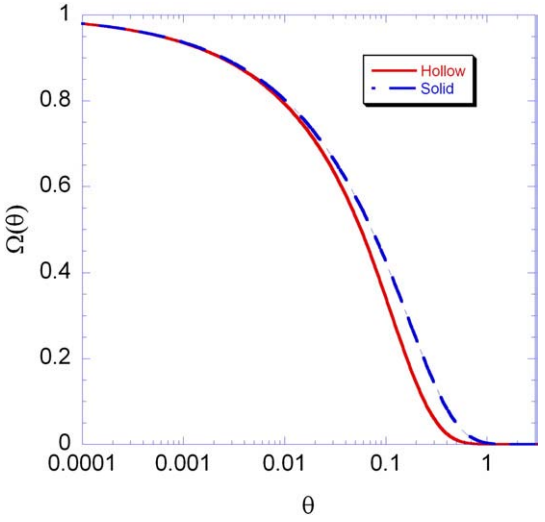

Fig. 1. Comparison of relaxation functions for solid and hollow cylinders. Note that the early behavior ($\theta<0.01$) is comparable for both functions. In this case $R_o/R_i=4$, which corresponds to a 10.2 cm (4 in) diameter cylinder with a 2.5 cm (1 in) diameter hole.

specimens, the re-expansion behavior occurs so rapidly that inadequate time is allowed for applying a static pressure. Specimens with high porosity or microcracking (such as routinely encountered in real structures) can exhibit a permeability several orders of magnitude higher than undamaged concrete with low porosity. Permeability values have been reported for concrete ranging over 8 orders of magnitude, from greater than 2×10^{-15} m^2 (for cracked concrete) [10] to less than 2×10^{-23} m^2 (for high performance concrete) [11].

In order to conveniently test cementitious specimens over a broad range of permeability, a hollow cylindrical specimen is considered for permeability testing. The primary advantage of the hollow cylinder geometry is the ability to measure the permeability of both high and low permeability specimens. Specimens with high permeability can be measured via radial flow-through by sealing the ends and applying a hydrostatic pressure to the outer radial face; this type of apparatus is demonstrated by Bhargava and Banthia [12]. The pressurized fluid will flow through the pore network from the outside in, and the associated fluid flux at the inner radial face can be measured. Though an SDP test could be used to test low permeability specimens, it is convenient to test the same hollow cylinder specimen in a dynamic pressurization test. The HDP test would consist of the measurement of the time-dependent axial strain of a hollow cylinder exposed to a constant hydrostatic pressure on both its inner and outer radial faces. Since the order of magnitude of permeability of a particular concrete specimen is not usually known a priori, a single hollow cylinder sample could be fabricated allowing for both radial flow-through and HDP testing. An additional advantage of the hollow cylinder geometry is that it will allow, for the first time, direct comparison of the measured permeability of cementitious materials determined from a flow-through test and a poromechanical test using the same specimen; results from such experiments will be presented in a future publication.

The objectives of the present study are to derive an approximate analytical solution in the time domain for the axial strain of a hollow cylinder during an HDP test in terms of the material permeability, and to validate that the permeability measured with the HDP technique yields comparable results to the SDP technique.

2. Theory

The theory behind the SDP technique was developed by Scherer [3]. The theory behind the HDP technique is similar, but has a few key differences.

The general solution for the axial strain in a hollow poroelastic cylinder has been derived by Kanj and Abousleiman [13,14] for boundary conditions identical to those presented by the problem of the HDP test;

$$\begin{array}{l} P(R_i,t)=H(t)P_A \\ P(R_o,t)=H(t)P_A \\ \langle\sigma_z(r,t)\rangle = -H(t)P_A \end{array}, \tag{1}$$

where $\langle\sigma_z(r,t)\rangle$ is the radial average of the axial stress and $H(t)$ is the Heaviside function, $P(t,r)$ is the pressure, P_A is the constant hydrostatic pressure applied at the boundary, t is the time, r is the radial coordinate, R_o is the outer radius, and R_i is the inner radius of the hollow cylinder. While the solution found by Kanj and Abousleiman may be used to solve the problem in the Laplace transform domain, it requires numerical inversion into the time domain. In order to devise a simple approximate solution in the time domain, it is useful to approach the problem in the same manner that Scherer [3] solved for the axial strain in a solid poroelastic cylinder exposed to hydrostatic pressure. The numerically inverted solution from Kanj and Abousleiman was utilized to fit the parameters in the appropriate analytical solution in the time domain derived herein. Viscoelastic relaxation of the materials was not considered since Scherer [3] demonstrated that such relaxation has a minimal effect on the axial strain history under the hydrostatic boundary conditions.

The poroelastic constitutive equation for the axial plane strain (ε_z) is

$$\varepsilon_z(t)=\frac{1}{E_p}\left\{\sigma_z(r,t)-\nu_p[\sigma_r(r,t)+\sigma_\theta(r,t)]\right\}+\varepsilon_f(r,t), \tag{2}$$

where σ_z, σ_r, and σ_θ are the axial, radial, and tangential stresses, E_p is the Young's modulus of the porous body, and ν_p is the Poisson's ratio of the porous body. The free strain is given by

$$\varepsilon_f(r,t)=\frac{bP(r,t)}{3K_p}, \tag{3}$$

where K_p is the bulk modulus of the drained porous body, and

$$b=1-\frac{K_p}{K_s} \tag{4}$$

is the Biot coefficient. K_s is the bulk modulus of the solid material skeleton. Assuming the pore fluid transport obeys Darcy's Law, the continuity equation may be expressed as

$$\frac{\dot{P}(r,t)}{M}+b\dot{\varepsilon}(r,t)=\frac{k}{\eta_L}\nabla^2P(r,t), \tag{5}$$

where k is the intrinsic permeability of the porous body (in dimensions of length squared), η_L is the pore fluid viscosity, ε is the volumetric strain, the overhead dots represent a partial time derivative, and

$$M=1/\left(\frac{\phi}{K_L}+\frac{b-\phi}{K_s}\right) \tag{6}$$

is the Biot modulus. K_L is the bulk modulus of the pore fluid and ϕ is the accessible liquid filled volumetric pore fraction of the porous body.

In this problem, we are considering a porous hollow cylinder that is pressurized hydrostatically. No fluid flow is allowed through the axial faces such that only radial flow is considered; therefore, Eq. (5) becomes

$$\frac{\dot{P}(r,t)}{M}+b\dot{\varepsilon}(r,t)=\frac{k}{\eta_L}\frac{1}{r}\frac{\partial}{\partial r}\left(r\frac{\partial P(r,t)}{\partial r}\right). \tag{7}$$

If we let $r = u(R_o - R_i)$ then Eq. (7) becomes

$$\frac{\dot{P}(u,t)}{M} + b\dot{\varepsilon}(u,t) = \frac{k}{\eta_L}\frac{1}{u(R_o - R_i)}\frac{\partial}{\partial[u(R_o - R_i)]}\left(u(R_o - R_i)\frac{\partial P(u,t)}{\partial[u(R_o - R_i)]}\right). \tag{8}$$

Based on the properties of differential operators, Eq. (8) simplifies to

$$\frac{\dot{P}(u,t)}{M} + b\dot{\varepsilon}(u,t) = \frac{k}{\eta_L(R_o - R_i)^2}\frac{1}{u}\frac{\partial}{\partial u}\left(u\frac{\partial P(u,t)}{\partial u}\right) \tag{9}$$

where $u = r/(R_o - R_i)$ is a dimensionless radial coordinate. As with a solid cylinder [3,15], the volumetric strain of a hollow cylinder exposed to an applied hydrostatic pressure P_A is

$$\varepsilon(u,t) = 3\beta\varepsilon_f + 3(1-\beta)\langle\varepsilon_f(t)\rangle - \frac{P_A}{K_p} \tag{10}$$

where $\langle\varepsilon_f(t)\rangle$ is the volumetric average of the free strain such that

$$\langle\varepsilon_f(t)\rangle = \frac{2}{R_o^2 - R_i^2}\int_{R_i}^{R_o}\varepsilon_f(r,t)rdr = \frac{2(R_o - R_i)}{R_o + R_i}\times\int_{R_i/(R_o - R_i)}^{R_o/(R_o - R_i)}\varepsilon_f(uR_o - uR_i,t)udu. \tag{11}$$

The constant β is defined according to [3] as

$$\beta = \frac{1+\nu_p}{3\left(1-\nu_p\right)}. \tag{12}$$

Eq. (10) may be obtained by recognizing that the poroelastic problem is analogous to the thermoelastic problem, and the free strain expressed in Eq. (2) is analogous to thermal strain. The stresses in the hollow cylinder, $\sigma_r(r,t)$, $\sigma_\theta(r,t)$, and $\sigma_z(r,t)$, can therefore be determined using the thermoelastic solution for a long, hollow cylinder [16] with the boundary conditions expressed in Eq. (1).

By combining Eqs.(3), (9), and (11) a partial differential equation for the pore pressure is obtained in the same form as for a solid cylinder,

$$\frac{\partial P(u,\theta)}{\partial\theta} + \left(\frac{(1-\beta)b\lambda}{1-(1-\beta)b\lambda}\right)\frac{\partial\langle P(\theta)\rangle}{\partial\theta} - \left(\frac{\lambda}{1-(1-\beta)b\lambda}\right)\frac{\partial P_A(\theta)}{\partial\theta} = \frac{1}{u}\frac{\partial}{\partial u}\left(u\frac{\partial P(u,\theta)}{\partial u}\right), \tag{13}$$

where

$$\lambda = \frac{Mb}{K_p + Mb^2}, \tag{14}$$

and the boundary conditions are expressed in Eq. (1). The reduced time is $\theta = t/\tau_v$, where τ_v is a relaxation time expressed as

$$\tau_v = \frac{\eta_L(R_o - R_i)^2}{k}\left(\frac{\beta b^2}{K_p} + \frac{1}{M}\right), \tag{15}$$

which normalizes the rate of pore pressure equilibration. In comparison to the relaxation time for the solid cylinder denoted in [3], the only difference in the expression for the relaxation time of the hollow cylinder is that the radius of the solid cylinder, R, is replaced by the term $(R_0 - R_i)$.

The goal of the following discussion is to illustrate a method for deriving an approximate analytical expression for τ_v as a function of $\varepsilon_z(t)$ in the time domain. Consider a step pressurization as a function of time, i.e.

$$P(R_i,t) = P(R_o,t) = H(t)P_A. \tag{16}$$

In this case, the axial strain immediately after the pressurization is

$$\varepsilon_z\left(t^{0+}\right) = -(1-b\lambda)\frac{P_A}{K_p}, \tag{17}$$

which is the same as for a solid cylinder. The final strain after pressurization is

$$\varepsilon_z(t\to\infty) = \frac{-P_A}{3K_s}, \tag{18}$$

which is also the same as for a solid cylinder. The time-dependent axial strain may therefore be expressed as

$$\varepsilon_z(\theta) = \varepsilon_z(\theta\to\infty) + \left\{\varepsilon_z\left(\theta^{0+}\right) - \varepsilon_z(\theta\to\infty)\right\}\Omega(\theta), \tag{19}$$

where $\Omega(\theta)$ is the compliance function. The Laplace transform of Eq. (19) is

$$\bar{\varepsilon}_z(s) = s\bar{\varepsilon}_z(s\to 0) + \{s\bar{\varepsilon}_z(s\to\infty) - s\bar{\varepsilon}_z(s\to 0)\}\bar{\Omega}(s) \tag{20}$$

where the overbars denote the Laplace transformed quantities, s is the transform variable, and the initial and final value theorems of Laplace transforms are used.

The function $\bar{\varepsilon}_z(s)$ was determined analytically in the Laplace transform domain using Kanj and Abousleiman's solution [14]. Then, by substituting $\bar{\varepsilon}_z(s)$ into Eq. (20), $\bar{\Omega}(s)$ was determined. The answer was inverted numerically into the θ domain with the Stehfest Algorithm [17] using the script from [18] in *Mathematica* [19] to obtain $\Omega(\theta)$. The relaxation functions for hollow and solid cylinders [3] are plotted in Fig. 1.

The important feature to recognize in Fig. 1 is that at short times ($\theta < 0.01$), the solid and hollow cylinder functions are virtually identical. The implication is that the short-time response of the hollow cylinder is able to be represented by the same function as the solid cylinder, shown by Scherer [3] to be

$$\Omega(\theta)\approx 1 - \frac{4}{\sqrt{\pi}}[1-(1-\beta)b\lambda]\sqrt{\theta}. \tag{21}$$

As a result, the relaxation function over the full time span can be approximated by a function of the form

$$\Omega(\theta)\approx\exp\left\{\frac{4}{\sqrt{\pi}}[1-(1-\beta)b\lambda]\left(\frac{\theta^m - \sqrt{\theta}}{1-\theta^n}\right)\right\} \tag{22}$$

where m and n are fit parameters. By plotting the relaxation function, $\Omega(\theta)$, associated with several different R_o/R_i ratios using Kanj and Abousleiman's solution numerically inverted into the θ domain, the functional dependence of m and n on R_o/R_i was determined. This dependence was fitted according to

$$m = 5.6152\left(\frac{R_o}{R_i}\right)^{-0.19623} \tag{23}$$

and

$$n = 0.40086 + 0.0056243\times\ln\left(\frac{R_o}{R_i}\right)^{1.8506}, \tag{24}$$

where the quality of the fits is illustrated in Figs. 2 and 3. The parameters m and n are weakly dependent on realistic material properties, but this dependence was neglected in favor of the stronger dependence on realistic values of R_o/R_i.

Fig. 4 shows the numerically inverted data generated using the solution of Kanj and Abousleiman for $\Omega(\theta)$ that has been fit with Eq. (22). Using fit parameters of $m = 4.4924$ and $n = 0.4235$, which correspond to $R_o/R_i = 4$, yielded an R^2 value of 0.99983.

In order to obtain the permeability of a given specimen, the strain versus time data must be obtained through testing, and then fit using Eq. (19). Eq. (22) must first be substituted into Eq. (19), and the appropriate m and n values obtained from Eqs. (23) and (24) must be

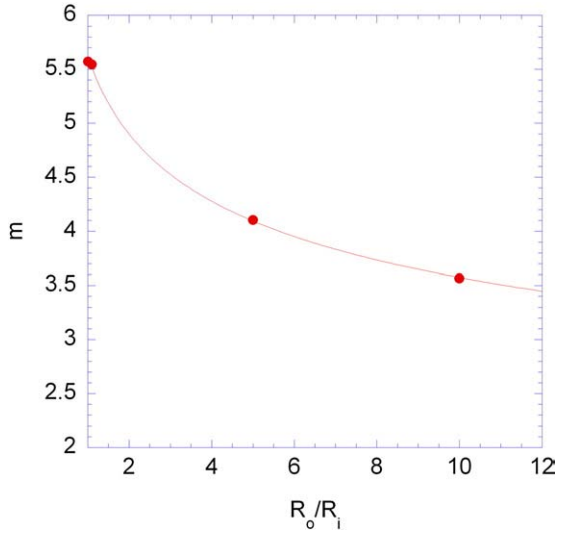

Fig. 2. The fit parameter m is determined by curve fitting several different radius ratios.

used to determine the value of τ_v from Eq. (19). Next, the values of η_L, R_o, and R_i can be entered directly into Eq. (15). β can be calculated according to Eq. (12) using 0.2 as an assumed value for ν_p. K_p and b can be determined from the strain history and Eq. (17) by first solving for K_s using Eq. (18), and then substituting Eqs. (14) and (4) into Eq. (17). M can be calculated using Eq. (6) by assigning a value to K_L (typically a textbook value — e.g. $K_L = 2.2$ GPa for water at room temperature) and either measuring or estimating ϕ. By substituting values of β, τ_v, K_p, M, b, η_L, R_o, and R_i into Eq. (15), the intrinsic permeability k may be determined directly.

3. Experimental

3.1. Materials

In this study, Vycor® glass and cement paste samples were tested for permeability using both SDP and HDP techniques. The Vycor® glass was type 7930 and was acquired in hollow tubes and solid cylindrical rods. The tubes and rods were 21 cm (8.2 in) long. The rods tested had a 6.4 mm (0.25 in) diameter and the tubes had an inner diameter of 1.9 cm (0.75 in) and an outer diameter of 2.1 cm (0.83 in). The rods and tubes were vacuum saturated in glycerol, a solution of glycerol and water, or pure distilled water prior to testing depending on the type of testing to be performed. The hollow cement paste samples were cast in 7.6×15 cm (3×6 in) cylinder molds while the solid specimens were cast in 3.7 cm (1.4 in) diameter tubes. The hollow specimens additionally had a 3.7 cm (1.4 in) diameter hole cast down the center through the length of the specimen. The cement used was a common Type I/II and was mixed at w/c of 0.5.

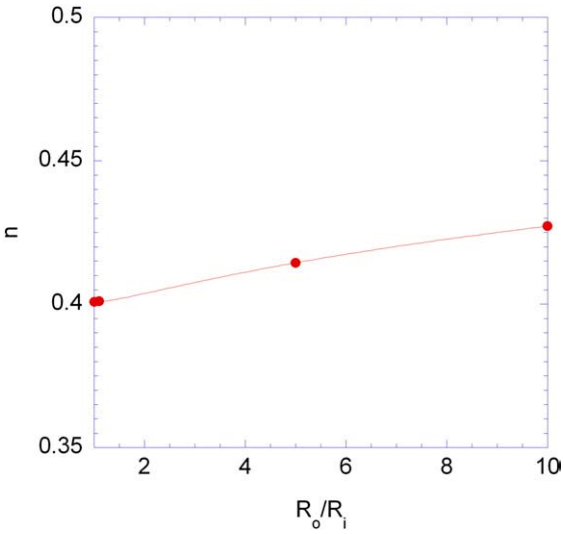

Fig. 3. The fit parameter n is determined by fitting the results of various radius ratios.

3.2. Specimen preparation

The cement paste was mixed according to ASTM C305-99. To achieve the hollow cylinder geometry, a thin walled polyethylene tube was glued into the center of the cylinder mold and a hole was cut in the center of the lid to accommodate this axial tube. Both the lid itself and the hole in the lid were sealed with silicone to prevent any moisture from leaving the cylinder during initial curing. The specimens were de-molded at approximately 12 h and were immediately placed in a saturated limewater solution to prevent any leaching of the internal calcium hydroxide. Additionally, the specimens in the limewater were placed under vacuum to promote saturation.

Soon after demolding, the specimens were trimmed on a diamond blade wet saw to ensure that their ends were uniform and parallel to one another. Approximately 12 h prior to testing with the HDP method, steel plates were glued onto the ends of the hollow cement paste specimens with a two-part marine epoxy to prevent any fluid from moving through the axial faces of the specimen and to facilitate mounting inside the testing apparatus. The Vycor® glass tubes would have been similarly sealed, but the thin wall thickness required caps that attached both to the ends as well as a small portion of the side of the tube. These caps were also secured with the marine epoxy. The ends of the solid rods were not sealed, but due to their extremely slender nature, a negligible amount of fluid would flow through the ends.

3.3. Porosity determination

One of the parameters necessary for determining k for both the SDP and HDP tests is the specimen porosity. Vichit-Vadakan and Scherer [20] show that porosity of cementitious materials determined by oven drying agrees with porosity measured by 2-propanol exchange and is much quicker. In this study, the oven drying technique was used for determining porosity. For the cement paste samples, this

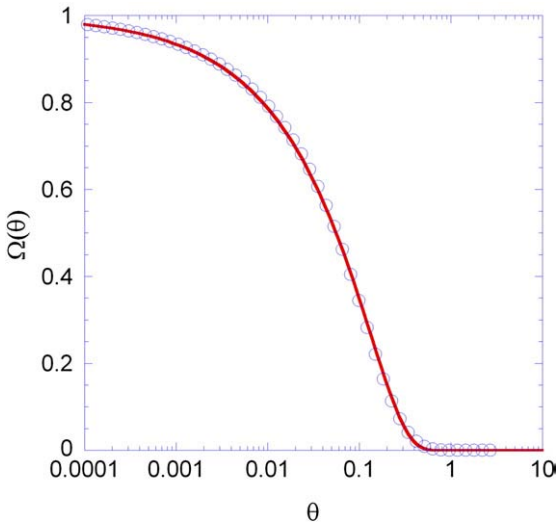

Fig. 4. Approximation of the relaxation function $\Omega(\theta)$ using Eq. (22). The discrete points are numerically inverted data for $\Omega(\theta)$ while the solid line is the approximate function. The function is evaluated using properties typical of concrete: $\beta = 1/2, b = 2/3, \lambda = 1/4$ with $R_o / R_i = 4$.

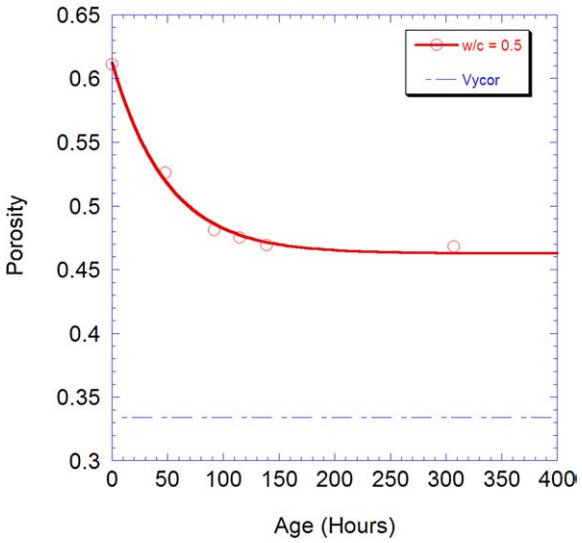

Fig. 5. The porosity of the cement paste specimens as a function of age.

method involved obtaining a small, representative disc of the material and saturating it under vacuum. The saturated surface dry weight and the dimensions of the sample were obtained using a digital balance capable of 0.001 g accuracy and a digital caliper with 0.001 cm accuracy. The sample was then placed in an oven at 110 °C. After drying overnight, the dry weight was obtained and the porosity was determined according to

$$\phi = \frac{M_{SSD} - M_{OD}}{V_{SSD} \times \rho_{Water}}, \tag{25}$$

where M_{SSD} is the mass in the saturated surface dry state, M_{OD} is the mass in the oven dry state, V_{SSD} is the measured volume in the saturated surface dry state, and ρ_{Water} is the density of water. The porosity of the Vycor® glass specimens was also determined using the oven drying technique.

The initial porosity of the cement paste was determined from the mix design, and then at subsequent ages with the oven drying technique to establish a best fit curve for each material. This curve was used to accurately estimate the porosity of a given specimen at a particular age. The porosity of the Vycor® glass was not time dependent and therefore was not tested at different ages. The cement paste porosity versus age plot is shown in Fig. 5 with an exponential fit. The porosity of the Vycor® glass is also shown in Fig. 5 for comparison purposes.

3.4. Hollow dynamic pressurization apparatus

The hollow dynamic pressurization apparatus involves a pressure chamber, in which the specimen is pressurized, that can withstand an internal pressure of 14 MPa (2000 psi). As shown in Fig. 6, the hollow specimen is attached to the top of the pressure chamber and is suspended in the fluid. The stainless steel linear variable differential transformer (LVDT) connecting rod runs through the hollow center of the specimen up to the LVDT coil. This LVDT system (also used in the

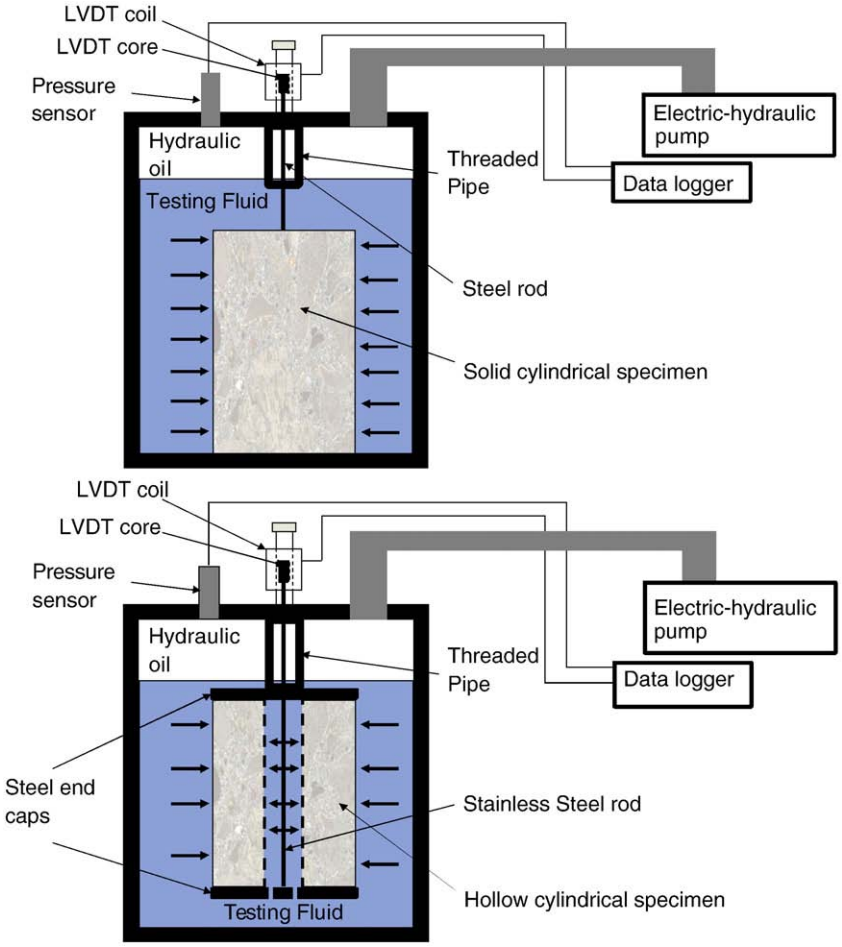

Fig. 6. The solid dynamic pressurization (top) and hollow dynamic pressurization (bottom) apparatuses use a pressure vessel and a non-contact LVDT system that measures the axial deformation of the specimen.

Table 1
Viscosities and bulk moduli of the fluids used for the HDP and SDP tests.

Fluid	Viscosity (Pa s)	K_L (Pa)
Distilled water	1.0×10^{-3}	2.2×10^{9}
65 wt.% glycerol	1.3×10^{-2}	3.6×10^{9}
90 wt.% glycerol	1.8×10^{-1}	4.2×10^{9}
Glycerol	1.1	4.5×10^{9}

SDP) is completely non-contact, which allows the chamber to be completely sealed with all electrical connections outside the chamber.

Hydrostatic pressure was applied using an electric hydraulic pump, which produced a relatively constant pressure that was regulated with a vented, inline pressure regulator. This setup allowed both pressurization and step depressurization, which is important to avoid high internal tensile stresses associated with a rapid release of the applied pressure [3]. The pressure was recorded with an electronic pressure sensor capable of 0.25% accuracy and was logged along with the displacement data using an electronic data logger.

3.5. Solid dynamic pressurization apparatus

The SDP apparatus is very similar to the hollow dynamic pressurization apparatus, but for a few key differences. The solid specimens rest on the bottom of the pressure chamber with the stainless steel LVDT connecting rod extending from the top of the specimen up to the LVDT coil as shown in Fig. 6. Since no end plates were used with the solid specimens, the LVDT connecting rod was attached to the top of the solid specimens directly. With the Vycor® rods, a small nut was threaded on and then glued to the LVDT connecting rod, and this nut was glued directly to the top surface of the Vycor® rod. For the cement paste, a small hole, slightly larger in diameter than the LVDT connecting rod, was drilled into the top of the specimen, to a depth of approximately 5 mm, and was then filled with marine epoxy. The rod was then fitted into this small hole and the epoxy was allowed to cure. This particular arrangement is necessary since there is no hollow center in the specimen through which to run the steel LVDT connecting rod.

4. Results

4.1. Permeability

In order to obtain the necessary inputs for the permeability calculations shown in Section 3, a few values, which are not obtained from either the SDP or HDP tests, must be determined. First, the dynamic viscosity of the particular pore fluid used must be determined. The viscosity of water is well characterized [21], and it does not change very much with small changes in temperature. However, glycerol varies substantially with a small change in temperature so the viscosity at laboratory temperature (~23 °C) was determined using a Brookfield rotational viscometer. The results of the viscosity testing are shown in Table 1 for pure glycerol as well as for blends of 65% glycerol and 90% glycerol (by weight) and water. Glycerol was chosen as a complimentary fluid to water for several reasons. First, the viscosity of glycerol is roughly 1000 times greater than that of water. The greater viscosity of the glycerol (and the glycerol–water blends) slowed the HDP and SDP testing of the Vycor® specimens so that adequate data collection could occur. In addition, glycerol and water are highly soluble in one another, which is critical for making fluid blends. Finally, the molecular size of glycerol is close to that of water (~5 Å for glycerol versus ~3 Å for water). The molecular size is of particular interest when considering the pore size of Vycor®. As noted by Vichat-Vidakan and Scherer [22], the molecular size of the testing fluid plays an important role in reducing the effective pore diameter as a result of an immobile adsorbed surface layer. Larger molecules would inhibit flow causing an artificially decreased permeability.

In order to facilitate the most direct comparison possible between the SDP and the HDP, two intermediate fluid blends were created with viscosities that fell in between that of water and pure glycerol. The viscosities of the blends were intentionally optimized to allow the SDP and HDP tests to run quickly while allowing time for adequate data collection and step pressurization of the pressure vessel. Water was used only for the SDP and the pure glycerol was only used for the HDP.

In addition to the viscosity, the bulk modulus, K_L, changes with each fluid. Though not as influential in the final permeability determination as the viscosity, K_L must be accurately estimated in order to obtain sensible permeability results. In the case of pure water and pure glycerol this determination involved using a reference value obtained from a source such as [21]. For the water/glycerol blends, the rule of mixtures,

$$K_{L-Blend} = f_1(K_{L-1}) + f_2(K_{L-2}), \tag{26}$$

was employed to estimate the bulk modulus of the blend where $K_{L\text{-}Blend}$ is the bulk modulus of the fluid blend, f_1 is the volume fraction of liquid 1, $K_{L\text{-}1}$ is the bulk modulus of liquid 1, $K_{L\text{-}2}$ is the bulk modulus of liquid 2,

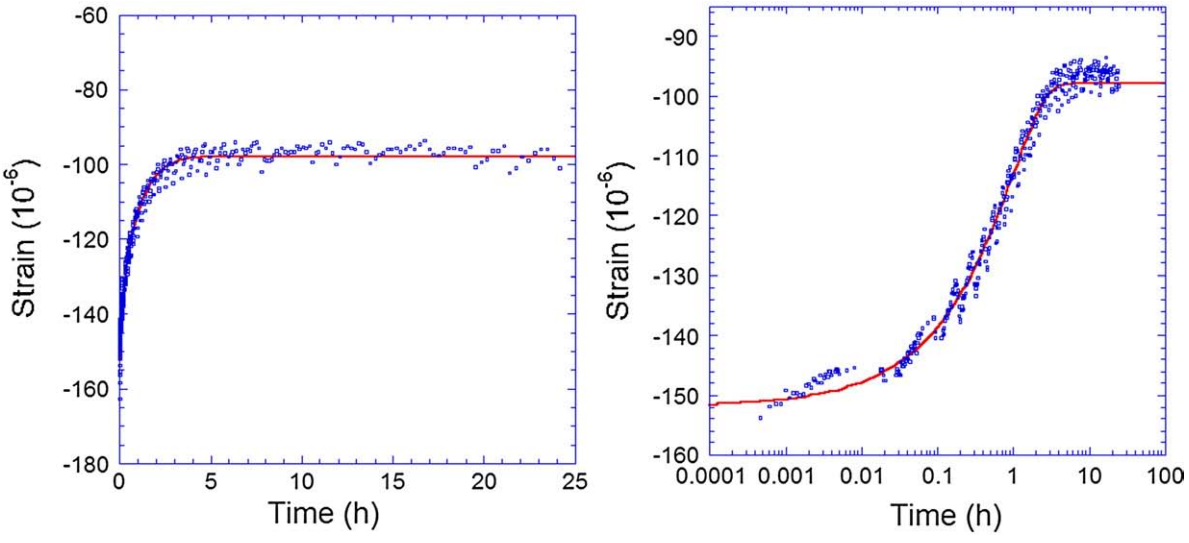

Fig. 7. Typical hollow dynamic pressurization strain data shown on time and log-time axes. The log-time axis more clearly shows when the specimen has fully relaxed.

Table 2
Measured Vycor® permeability (using various fluids) and associated statistical quantities.

Trial	Hollow DP results			Solid DP results	
	Permeability (nm^2)			Permeability (nm^2)	
	Glycerol	65 wt.%	90 wt.%	Glycerol	65 wt.%
1	0.021	0.018	0.023	0.038	0.008
2	0.024	0.019	0.030	0.011	0.013
3	0.020	0.015	0.026	0.013	0.012
4	0.032	0.018	0.021	0.024	0.009
5	0.014	0.015	0.021	0.024	0.008
6	0.028	0.017	0.021	0.031	0.009
7	0.034	0.019	0.023	0.019	0.014
8	0.019	0.023	0.020	0.035	0.016
9		0.018	0.017		0.018
10		0.019	0.015		0.018
11			0.016		
Average	0.024	0.018	0.021	0.024	0.012
Standard deviation	0.0069	0.0023	0.0044	0.0098	0.0041
Coefficient of variation	28%	13%	21%	40%	33%
Combined coefficient of variation		24%		53%	

and f_2 is the volume fraction of liquid 2. The bulk moduli of the various liquids used in both the HDP and the SDP test are shown in Table 1.

The final input parameter required for calculating permeability for both the SDP and HDP techniques is the strain-time history under a constant hydrostatic pressure, which can be fit to determine the relaxation time, τ_v, and ultimately the permeability of the material. Fig. 7 shows a typical strain-time history for the HDP test, shown on both the time and log-time axes. These results are for a hollow Vycor® tube tested in pure glycerol. The plots show that equilibrium is reached in approximately 9 h, which is roughly equivalent to the fit parameter τ_v.

4.1.1. Vycor®

The results from the testing of hollow and solid Vycor® specimens for permeability show good correlation between the HDP and the SDP techniques. The difference between the average permeability determined from the HDP and the SDP is 13%. The permeability values for the Vycor® specimens are presented in Table 2.

Typical concrete permeability tests show high variability between repetitions. Banthia and Mindess report coefficients of variation between 62% and 112% [12] while Bhargava and Banthia report a coefficient of variation of 65% [23]. With the HDP and the SDP techniques, the greatest coefficient of variation was 40%, and the greatest combined coefficient of variation was 53%. Additionally, the results shown in Table 2 agree reasonably well with the Vycor® permeability results obtained by Vichit-Vidakan and Scherer [22] (both in mean and in standard deviation), as well as with the modeled permeability results for Vycor® obtained by Bentz et al. [24].

When evaluating the agreement in means of two data sets, the Student's *T*-test is frequently employed. For this test a characteristic '*t*' statistic is calculated according to

$$t = \frac{\mu_1 - \mu_2 - \Delta}{\sqrt{\frac{s_1^2}{m} + \frac{s_2^2}{n}}}, \tag{27}$$

where μ_1 is the mean of the first data set, μ_2 is the mean of the second data set, Δ is the null value, s_1 is the standard deviation of the first data set, s_2 is the standard deviation of the second set, m is the number of data points in the first data set, and n is the number of data points in the second set [25]. This '*t*' value is compared to a reference value based on the confidence level and the number of data points in the combined data set. Typically, results are tested at the 95% confidence level, which means that the hypothesized correlation is predicted to be correct 95% of the time. By using the reference value corresponding to the 95% confidence level and the appropriate number of data points, the null value Δ can be determined. Once the Δ value is obtained the percent difference can be determined according to,

$$\%\text{percent difference} = \frac{\Delta}{(\mu_1 + \mu_2)/2} \times 100. \tag{28}$$

With the data presented in Table 2, it can be shown that the percent difference in the permeability values from the HDP test and the SDP test will be 17% or less 95% of the time.

From a practical perspective, the percent difference between the Vycor® glass permeability measured using the SDP technique and the HDP technique is insignificant. Therefore, the HDP test has been successfully validated and has been shown to yield the same permeability as the SDP test for Vycor® glass.

4.1.2. Cementitious materials

In order to generate the most direct comparison possible, the HDP and the SDP methods were performed on hollow and solid cement paste specimens beginning approximately 90 h after the specimens were cast. Specifically, a hollow specimen was tested in one pressure vessel and a solid specimen in a companion pressure vessel, with the test beginning at effectively the same moment. At these early ages, many test repetitions could be obtained in a reasonably short period of time. By simultaneously testing these samples, the effect of any age differences between specimens was avoided since the solid sample was the same age as the hollow sample and vice versa. Since the hollow and solid specimens were cast from the same mix, and were tested at an identical age, the permeability results from the two tests can be readily compared at a given age to evaluate the new HDP method.

To help illustrate the sensitivity of the HDP method for discerning the permeability of different materials, the permeability results of a slightly different material are compared to those results obtained in this study. Cement pastes with w/c of 0.5 and 0.6 were tested by Vichat-Vidakan and Scherer [20] using the beam bending (BB) technique; the results are plotted along with the results obtained in this study using the HDP and SDP techniques in Fig. 8.

The difference between a low permeability material and a high permeability material is worth noting. The difference between a 0.5 w/c paste and a 0.6 w/c paste is reported as a full order of magnitude (i.e. 0.001 nm^2 as compared to 0.01 nm^2) by Grasley et al. [2]; this

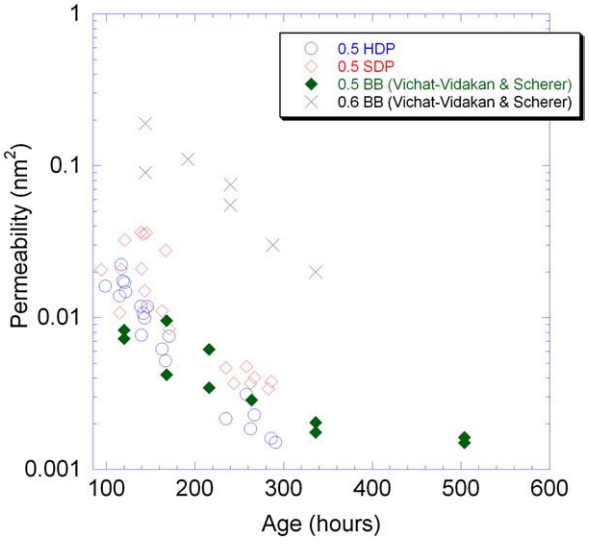

Fig. 8. The results of the hollow dynamic pressurization test and the solid dynamic pressurization tests shown as a function of age. For comparison purposes, the results from another study [20] are included.

difference in measured permeability is a change of 900%. The maximum difference in the average measured permeability values reported in Table 2 is 53%, which is well less than an order of magnitude, indicating that the HDP test is sufficiently sensitive to discern the permeability of the two different materials.

From Fig. 8, it appears that the results from the BB technique compare favorably with those of the HDP technique. However, the results from the HDP technique tend to be consistently slightly lower than for the SDP technique. It is hypothesized that the differences arise from two possible sources. First, the greater pressurized boundary surface area in the hollow cylinder may result in a lower measured permeability due to a decreased permeability in the exposed surface layer. As mentioned in Section 4, the specimens were placed in a saturated lime solution immediately after demolding, and were maintained in that solution indefinitely. It was observed that the surfaces of the specimens in the solution would tend to have a covering of calcium hydroxide crystals, which may have slightly reduced the penetrability of the surface layers in the specimens. Ye [26] speculated that a surface covering of calcium hydroxide can block entry of water into the pore network, altering the measured permeability. Second, since the solid cylinders were slender (length/diameter ratio $\approx$6), the ends of the cylinders were not sealed. Intrusion of water through the ends of the cylinder may have slightly increased the measured permeability of the solid cylinder. Both the top and bottom faces of the hollow cylinder were sealed.

Although the permeability test conditions for cementitious materials discussed in the literature differ from those in this experimental study, comparison of the permeability values obtained in other tests on similar materials provides useful context into which the results from this study may be placed. As mentioned above, Vichat-Vidakan and Scherer tested cement paste permeability [20] with the beam bending technique at early ages using a Type III cement with a 0.5 w/c (results shown in Fig. 8). Furthermore, Grasley et al. [2] used the SDP technique to measure the permeability of cement paste with w/c of 0.5 (Type III cement) at early ages, and reported permeabilities of about 0.08 nm^2 (3 d age) to 0.001 nm^2 (>28 d age). Results from these poromechanical techniques with identical w/c ratios show excellent agreement to the values obtained in this study. Nyame and Illston [27] report permeability values ranging from about 30 nm^2 (4 d age) to about 0.007 nm^2 (28 d age) for cement paste with w/c of 0.47 determined using a flow-through permeameter. Additionally, Mindess and Young [28] report permeability values ranging from about 100 nm^2 (5 d age) to about 0.006 nm^2 (28 d age) for a 0.51 w/c using a flow-through permeameter. Ye [26] measured permeability values ranging from about 90 nm^2 (at 3 d age) to about 0.1 nm^2 (at 28 d age) with a flow through test. The flow-through results from the literature are higher than the results from poromechanical techniques on similar materials, indicating the need for direct comparison of the two techniques on the same material in a controlled experimental program in order to verify their equivalence.

5. Conclusions

Results from the new HDP test for evaluating material permeability have been successfully correlated to results from the SDP test. Comparison of the permeability results of the HDP test and the SDP test on Vycor® glass samples effectively validated the new HDP test, while the comparison of permeability results using cement paste further reinforced the assertion that the HDP test is a valid tool to evaluate permeability in cementitious materials. The hollow cylinder geometry allows for HDP testing as well as radial flow-through permeability testing such that cementitious materials with a broad range of permeabilities can be tested with a single apparatus. Future work will include extending the HDP testing to realistic concrete materials, and a direct comparison of HDP permeability results with permeability determined using a radial flow-through technique. Additionally, the relationship between aggregate size and the minimum thickness of a hollow cylinder required to obtain representative permeability will be investigated.

Acknowledgements

The authors thank the reviewers and editor for their comments and suggestions, which significantly improved the final manuscript.

References

[1] A. Neville, Suggestions of research areas likely to improve concrete, Concr Int 18 (5) (1996) 44–49.
[2] Z.C. Grasley, G.W. Scherer, D.A. Lange, J.J. Valenza, Dynamic pressurization method for measuring permeability and modulus: II. Cementitious materials, Mater Struct 40 (7) (2007) 711–721.
[3] G.W. Scherer, Dynamic pressurization method for measuring permeability and modulus: I. Theory, Mater Struct 39 (294) (2006) 1041–1057.
[4] G. Ye, P. Lura, K. Van Breugel, Modelling of water permeability in cementitious materials, Mater Struct 39 (293) (2006) 877–885.
[5] G.W. Scherer, Poromechanics analysis of a flow-through permeameter with entrapped air, Cem Concr Res 38 (3) (2008) 368–378.
[6] R.D. Hooton, Permeability and Pore Structure of Cement Pastes Containing Flyash, Slag, and Silica Fume, ASTM, Denver, CO, USA, 1986 Philadelphia, PA, USA.
[7] G.W. Scherer, J.J. Valenza II, G. Simmons, New methods to measure liquid permeability in porous materials, Cem Concr Res 37 (3) (2007) 386–397.
[8] G.W. Scherer, Measuring permeability of rigid materials by a beam-bending method: I, Theory, J Am Ceram Soc 83 (9) (2000) 2231–2239.
[9] G.W. Scherer, Thermal expansion kinetics: method to measure permeability of cementitious materials. I. Theory, J Am Ceram Soc 83 (11) (2000) 2753–2761.
[10] C.M. Aldea, S.P. Shah, A. Karr, Permeability of cracked concrete, Mater Struct 32 (219) (1999) 370–376.
[11] A.S. El-Dieb, R.D. Hooton, Water-permeability measurement of high performance concrete using a high-pressure triaxial cell, Cem Concr Res 25 (6) (1995) 1199–1208.
[12] A. Bhargava, N. Banthia, Measurement of concrete permeability under stress, Exp Tech 30 (5) (2006) 28–31.
[13] Y.N. Abousleiman, M.Y. Kanj, The generalized Lame Problem-part II: applications in poromechanics, J Appl Mech 71 (2) (2004) 180–189.
[14] M.Y. Kanj, Y.N. Abousleiman, The generalized lame problem — Part I: coupled poromechanical solutions, J Appl Mech 71 (2) (2004) 168–179.
[15] J. Gross, G.W. Scherer, Dynamic pressurization: novel method for measuring fluid permeability, J Non-Cryst Solids 325 (1–3) (2003) 34–47.
[16] H.H. Sherief, A.E.M. Elmisiery, M.A. Elhagary, Generalized thermoelastic problem for an infinitely long hollow cylinder for short times, J Therm Stresses 27 (10) (2004) 885–902.
[17] H. Stehfest, Numerical inversion of Laplace transforms, Commun ACM 13 (1) (1970) 47–49.
[18] A. Mallet. 2000, University of Mauritius.
[19] Mathematica. 2007, Wolfram Research Inc.: Champaign, IL.
[20] W. Vichit-Vadakan, G.W. Scherer, M. Grutzeek, Measuring permeability of rigid materials by a beam-bending method: III, cement paste, J Am Ceram Soc 85 (6) (2002) 1537–1544.
[21] B.R. Munson, D.F. Young, T.H. Olkiishi, Fundamentals of Fluid Mechanics, 4th edJohn Wiley and Sons Inc, 2002.
[22] W. Vichit-Vadakan, G.W. Scherer, Measuring permeability of rigid materials by a beam-bending method: II. Porous glass, J Am Ceram Soc 83 (9) (2000) 2240–2245.
[23] A. Bhargava, N. Banthia, Permeability of concrete with fiber reinforcement and service life predictions, Mater Struct 41 (2) (2008) 363–372.
[24] D.P. Bentz, E.J. Garboczi, D.A. Quenard, Modelling drying shrinkage in reconstructed porous materials: application to porous Vycor glass, Modell Simul Mater Sci Eng 6 (3) (1998) 211–236.
[25] J.L. Devore, Probability and Statistics, 6 edBrooks/Cole-Thompson Learning, Belmont, Ca, 2004.
[26] G. Ye, The Microstructure and Permeability of Cementitious Materials, Delft University, Delft, The Netherlands, 2003.
[27] B.K. Nyame, J.M. Illston, Relationships between permeability and pore structure of hardened cement paste, Mag Concr Res 33 (116) (1981) 139–146.
[28] S. Mindess, J.F. Young, Concrete, Prentice Hall, Englewood Cliffs, NJ, 1981.